Supplement of Atmos. Chem. Phys., 24, 13849–13864, 2024
https://doi.org/10.5194/acp-24-13849-2024-supplement

Atmospheric Chemistry and Physics
Open Access
EGU

Supplement of

Aerosol hygroscopicity over the southeast Atlantic Ocean during the biomass burning season – Part 1: From the perspective of scattering enhancement

Lu Zhang et al.

Correspondence to: Michal Segal-Rozenhaimer (segalrozenhaimer@baeri.org) and Haochi Che (haochi.che@geo.uio.no)

S1. Minor contribution of super-micron particles to the total scattering

The PNSD of super-micron particles was measured by an aerodynamic particle sizer (APS), whose aerodynamic diameter was converted to the volume equivalent diameter according to DeCarlo et al. (2004). Particles were assumed to be spherical (shape factor = 1) with a density of 1.5 g cm^{-3}. The dry total scattering coefficients at 540 nm were measured by Radiance Research M903 integrating nephelometer.

We calculated the scattering coefficient of super-micron particles at 540 nm using the Mie model, with inputs being the PNSD from APS and a refractive index of 1.51+0.0048i for dust (Di Biagio et al., 2019). We have also calculated the scattering coefficient using the refractive index of sea salt and the results are similar to those using the refractive index of dust; therefore, not shown here. The ratio of the scattering coefficient of super-micron particles to the total scattering coefficient reflects the contribution of super-micron particles to the total scattering. The distribution of the ratio is shown in Fig. S1. As illustrated in the figure, 85% of the data have a ratio of less than 0.015, indicating that the contribution of super-micron particles to the total scattering is less than 1.5% for 85% of the cases, demonstrating the minimal impact of super-micron particles on the total scattering.

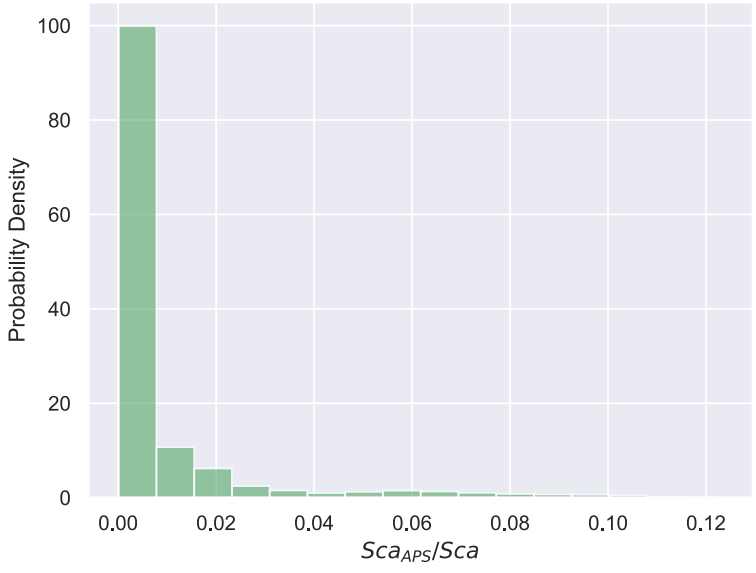

Figure S1. The PDF distribution of the ratio (Sca_{APS}/Sca) of the scattering coefficient of super-micron particles to the total scattering coefficient.

S2. Sensitivity of *f*(RH) to PNSD

The $\gamma(\mathrm{Fo},\kappa_{\mathrm{OA}},\mathrm{BCr})$ parameterization was obtained assuming mean PNSD with the geometric mean diameter D_{gn}=150 nm and standard deviation σ_{sg}=1.6. To evaluate the sensitivity of *f*(RH) to PNSD and explore its applicability to broader regions, we calculated the γ with various D_{gn} and σ_{sg} and compared it to those with the mean PNSD. Results are shown in Fig. S2 taking measurements in ORACLES 2018 as an example. The deviations of γ calculated with D_{gn} and σ_{sg} in their interquartile ranges and the 10^{th} - 90^{th} percentile ranges are both smaller than 2% and 3%, respectively, indicating a minor influence of PNSD to $\gamma(\mathrm{Fo},\kappa_{\mathrm{OA}},\mathrm{BCr})$ parameterization and supporting the application of $\gamma(\mathrm{Fo},\kappa_{\mathrm{OA}},\mathrm{BCr})$ parameterization to ORACLES 2018. For a broader aerosol population, the deviation is found to be less than 5% when D_{gn} varies from 75 nm to 210 nm (approx. -50% to 35% deviated from the mean D_{gn}) and smaller than 10% with σ_{sg} varying from 1.25 to 1.9 (approx. ±20% deviated from the mean σ_{sg}). The broad ranges of D_{gn} and σ_{sg} suggest that the $\gamma(\mathrm{Fo},\kappa_{\mathrm{OA}},\mathrm{BCr})$ parameterization can be applied to broader aerosol populations (Hussein et al., 2004; Shen et al., 2015). Caution is needed when Aitken mode aerosols are dominant such as new particle formation events, as the deviation of γ increases sharply for D_{gn} smaller than 75 nm or σ_{sg} less than 1.25 (Fig. S1). We believe this parameterization would benefit investigations of aerosol direct radiative forcing, aerosol liquid water content, comparison and evaluation of remote sensing and in situ measurements, and visibility degradation.

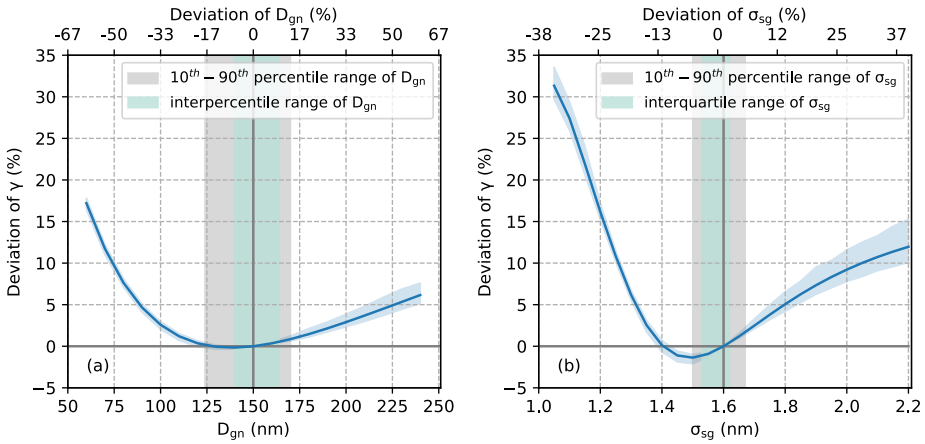

Figure S2. The sensitivity of γ to PNSD. (a) Deviation of γ predicted with various geometric mean diameters D_{gn} to that with the mean D_{gn} in ORACLES 2018 and (b) deviation of γ predicted with various standard deviation σ_{sg} to that with the mean σ_{sg} in ORACLES 2018. Blue lines represent

the mean value, and the blue shaded areas represent the 99.7% confidence interval (mean±3 standard deviation). The green and grey shaded areas represent the 25th to 75th percentile and the 10th to 90th percentile of D_{gn} or σ_{sg}, respectively, in ORACLES 2018. The upper x-axis shows the deviation of D_{gn} or σ_{sg} to its mean values in ORACLES 2018.

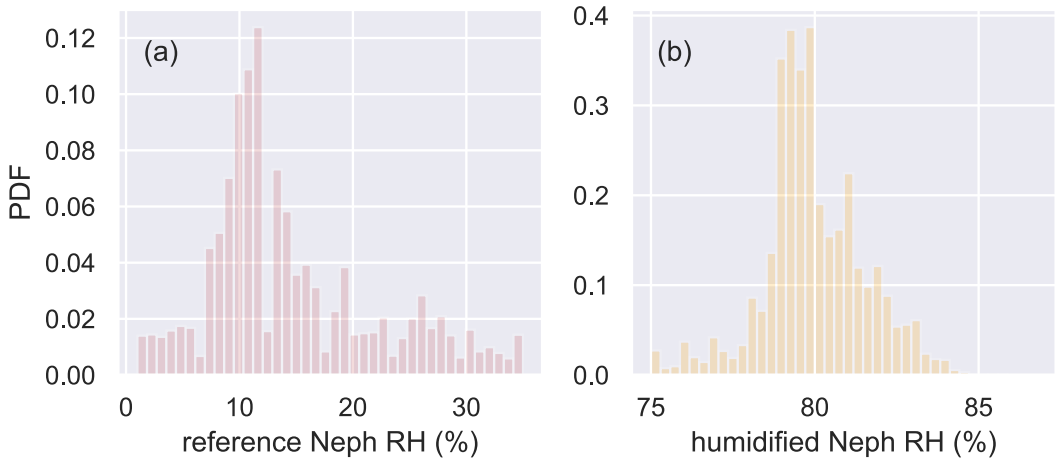

Figure S3. Distributions of the RHs for reference and humidified Nephs during the campaign.

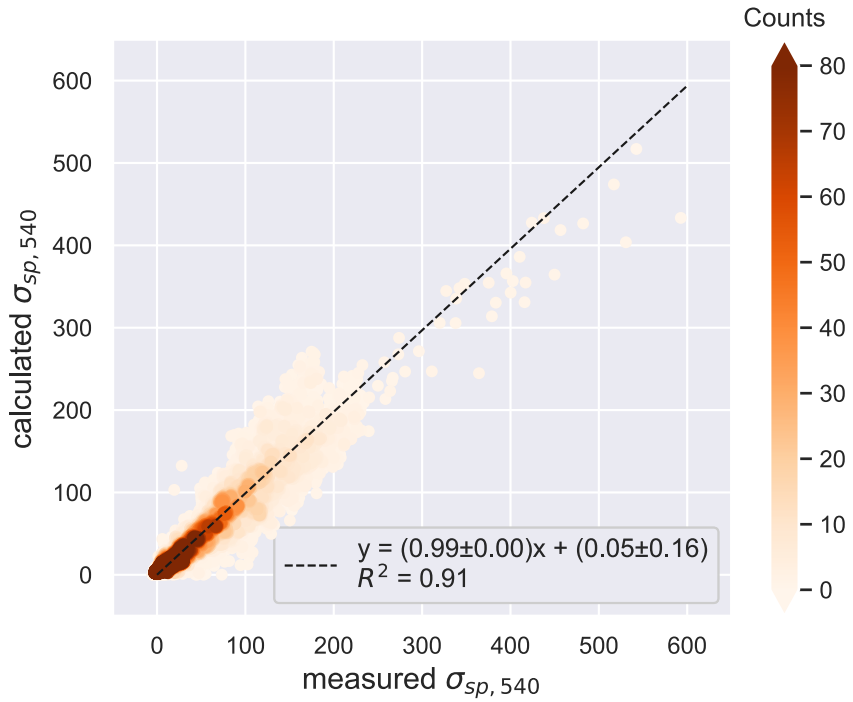

Figure S4. Calculated and measured scattering coefficients under dry conditions, colored by the count of data in each dot.

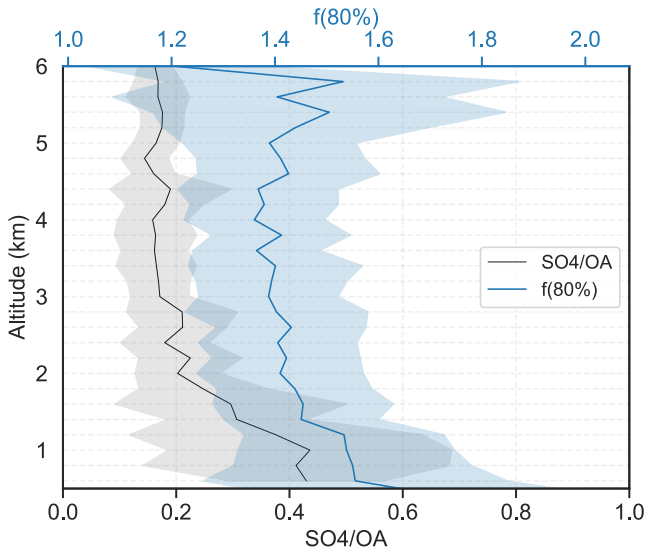

Figure S5. Vertical distributions of SO_4/OA and f(80%) in 2016 and 2018 ORACLES campaigns. The lines are the mean value in every 200 m bin. Shadings represent the standard deviation in every 200 m bin.

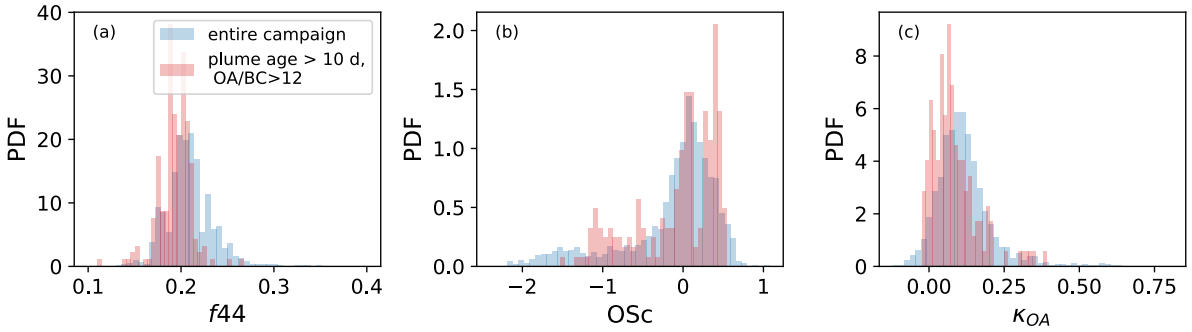

Figure S6. PDF of f44, OSc, and κ_{OA} for the entire 2016 and 2018 ORACLES campaign and for aerosols with plume age > 10 days and OA/BC>12.

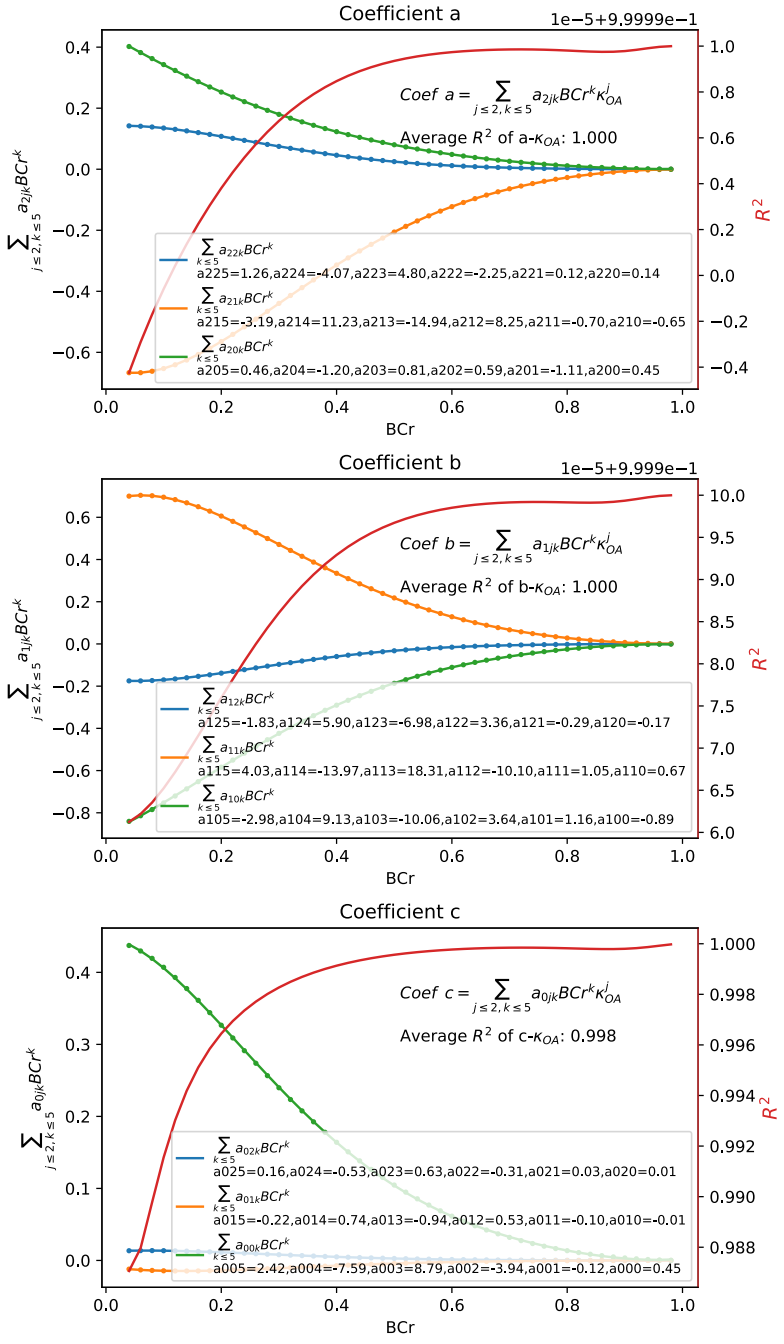

Figure S7. Coefficients a, b, and c of the second-order polynomial fit M(Fo,κ_{OA},BCr) = aFo^2+bFo+c. The a, b, and c can be further fitted into a second-order polynomial fit of κ_{OA} with coefficients being $\sum_{\substack{j\le 2\\ k\le 5}} a_{2jk}BCr^k$, $\sum_{\substack{j\le 2\\ k\le 5}} a_{1jk}BCr^k$, and $\sum_{\substack{j\le 2\\ k\le 5}} a_{0jk}BCr^k$, respectively. Red lines represent the correlation coefficient R^2 of the quadratic relationship between a, b, and c with κ_{OA}

under each BCr, average values are shown in the texts. These coefficients are fitted into a fifth-order polynomial equation with BCr with coefficients shown in each legend.

Table S1. Density (ρ), refractive index ($m=n+ik$) at 540 nm, and hygroscopicity parameter (κ) of inorganics, OA, and BC used in this study.

	$(NH_4)_2SO_4$	NH_4HSO_4	NH_4NO_3	KCl	OA	BC
ρ (g cm^{-3})	1.77 (Lide, 2008)	1.78 (Lide, 2008)	1.72 (Lide, 2008)	1.98 (Kuang et al., 2021)	1.4 (Alfarra et al., 2006)	1.8 (Bond and Bergstrom, 2006; Liu et al., 2017)
$m=n+ik$	1.45[a]	1.44[a]	1.56[a]	1.46[a]	1.65 (Feng et al., 2013)	1.95+0.79i (Bond and Bergstrom, 2006; Liu et al., 2021)
κ	0.47 (Topping et al., 2005; Gysel et al., 2007; Kim et al., 2020)	0.56 (Kuang et al., 2021)	0.58 (Topping et al., 2005; Gysel et al., 2007; Kim et al., 2020)	0.89 (Kuang et al., 2021)	n/a[b]	0 (Kuang et al., 2021; Topping et al., 2005; Gysel et al., 2007)

[a] Aerosol Refractive Index Archive from http://eodg.atm.ox.ac.uk/ARIA/ based on Cotterell et al. (Cotterell et al., 2017) and Querry (Querry, 1985); [b] k_{OA} is determined in the study.

Table S2. The mean and standard deviation of aerosol hygroscopicity related parameters.

	2016		2018	
	>2 km	<2 km	>2 km	<2 km
f(80%)	1.41±0.18	1.51±0.23	1.38±0.15	1.50±0.15
$\kappa_{f(RH)}$	0.22±0.07	0.23±0.09	0.18±0.07	0.21±0.06
κ_{OA}	0.11±0.09	0.14±0.11	0.10±0.06	0.15±0.05
SO4(%)	10.0±2.9	19.7±9.3	13.3±3.7	18.9±5.4
OA(%)	67.5±5.9	60.1±9.6	65.7±4.0	51.6±9.2
Age (d)	7.2±2.6	8.6±1.8	6.3±1.2	9.3±1.4
f44	0.21±0.03	0.22±0.03	0.21±0.02	0.24±0.03

Table S3. Parameterization coefficients of M(Fo,κ_{OA},BCr) and γ(Fo,κ_{OA}=0,BCr) in Eq. 4 and 5. Columns are the subscripts of parameter a. a_{X5} with X of 00 represents a_{005} (i=0, j=0, k=5) used in Eq. 5.

Subscript X	a_{X5}	a_{X4}	a_{X3}	a_{X2}	a_{X1}	a_{X0}
00	2.42	-7.59	8.79	-3.94	-0.12	0.45
01	-0.22	0.74	-0.94	0.53	-0.10	-0.01
02	0.16	-0.53	0.63	-0.31	0.03	0.01
10	-2.98	9.13	-10.06	3.64	1.16	-0.89
11	4.03	-13.97	18.31	-10.10	1.05	0.67
12	-1.83	5.90	-6.98	3.36	-0.29	-0.17
20	0.46	-1.20	0.81	0.59	-1.11	0.45
21	-3.19	11.23	-14.94	8.25	-0.70	-0.65
22	1.26	-4.07	4.80	-2.25	0.12	0.14
0	0.83	-3.13	4.44	-2.66	-0.14	0.67
1	0.61	-1.94	2.56	-1.90	1.33	-0.66
2	-1.25	4.48	-6.31	4.21	-1.13	-0.00

$$M(Fo, \kappa_{OA}, BCr)$$

$$= \begin{bmatrix} Fo^2 & Fo & 1 \end{bmatrix} \begin{bmatrix} \begin{bmatrix} {\kappa_{OA}}^2 & \kappa_{OA} & 1 \end{bmatrix} \left(\begin{bmatrix} a_{225} & a_{224} & a_{223} & a_{222} & a_{221} & a_{220} \\ a_{215} & a_{214} & a_{213} & a_{212} & a_{211} & a_{210} \\ a_{205} & a_{204} & a_{203} & a_{202} & a_{201} & a_{200} \end{bmatrix} \begin{bmatrix} BCr^5 \\ BCr^4 \\ BCr^3 \\ BCr^2 \\ BCr \\ 1 \end{bmatrix} \right) \\ \begin{bmatrix} {\kappa_{OA}}^2 & \kappa_{OA} & 1 \end{bmatrix} \left(\begin{bmatrix} a_{125} & a_{124} & a_{123} & a_{122} & a_{121} & a_{120} \\ a_{115} & a_{114} & a_{113} & a_{112} & a_{111} & a_{110} \\ a_{105} & a_{104} & a_{103} & a_{102} & a_{101} & a_{100} \end{bmatrix} \begin{bmatrix} BCr^5 \\ BCr^4 \\ BCr^3 \\ BCr^2 \\ BCr \\ 1 \end{bmatrix} \right) \\ \begin{bmatrix} {\kappa_{OA}}^2 & \kappa_{OA} & 1 \end{bmatrix} \left(\begin{bmatrix} a_{025} & a_{024} & a_{023} & a_{022} & a_{021} & a_{020} \\ a_{015} & a_{014} & a_{013} & a_{012} & a_{011} & a_{010} \\ a_{005} & a_{004} & a_{003} & a_{002} & a_{001} & a_{000} \end{bmatrix} \begin{bmatrix} BCr^5 \\ BCr^4 \\ BCr^3 \\ BCr^2 \\ BCr \\ 1 \end{bmatrix} \right) \end{bmatrix} \quad \text{(S1)}$$

$$\gamma(Fo, \kappa_{OA} = 0, BCr) = \begin{bmatrix} Fo^2 & Fo & 1 \end{bmatrix} \left(\begin{bmatrix} a_{25} & a_{24} & a_{23} & a_{22} & a_{21} & a_{20} \\ a_{15} & a_{14} & a_{13} & a_{12} & a_{11} & a_{10} \\ a_{05} & a_{04} & a_{03} & a_{02} & a_{01} & a_{00} \end{bmatrix} \begin{bmatrix} BCr^5 \\ BCr^4 \\ BCr^3 \\ BCr^2 \\ BCr \\ 1 \end{bmatrix} \right) \quad \text{(S2)}$$

References

Alfarra, M. R., Paulsen, D., Gysel, M., Garforth, A. A., Dommen, J., Prévôt, A. S. H., Worsnop, D. R., Baltensperger, U., and Coe, H.: A mass spectrometric study of secondary organic aerosols formed from the photooxidation of anthropogenic and biogenic precursors in a reaction chamber, Atmospheric Chem. Phys., 6, 5279–5293, https://doi.org/10.5194/acp-6-5279-2006, 2006.

Bond, T. C. and Bergstrom, R. W.: Light Absorption by Carbonaceous Particles: An Investigative Review, Aerosol Sci. Technol., 40, 27–67, https://doi.org/10.1080/02786820500421521, 2006.

Cotterell, M. I., Willoughby, R. E., Bzdek, B. R., Orr-Ewing, A. J., and Reid, J. P.: A complete parameterisation of the relative humidity and wavelength dependence of the refractive index of

hygroscopic inorganic aerosol particles, Atmospheric Chem. Phys., 17, 9837–9851, https://doi.org/10.5194/acp-17-9837-2017, 2017.

Feng, Y., Ramanathan, V., and Kotamarthi, V. R.: Brown carbon: a significant atmospheric absorber of solar radiation?, Atmospheric Chem. Phys., 13, 8607–8621, https://doi.org/10.5194/acp-13-8607-2013, 2013.

Gysel, M., Crosier, J., Topping, D. O., Whitehead, J. D., Bower, K. N., Cubison, M. J., Williams, P. I., Flynn, M. J., McFiggans, G. B., and Coe, H.: Closure study between chemical composition and hygroscopic growth of aerosol particles during TORCH2, Atmospheric Chem. Phys., 7, 6131–6144, https://doi.org/10.5194/acp-7-6131-2007, 2007.

Hussein, T., Puustinen, A., Aalto, P. P., Mäkelä, J. M., Hämeri, K., and Kulmala, M.: Urban aerosol number size distributions, Atmospheric Chem. Phys., 4, 391–411, https://doi.org/10.5194/acp-4-391-2004, 2004.

Kim, N., Yum, S. S., Park, M., Park, J. S., Shin, H. J., and Ahn, J. Y.: Hygroscopicity of urban aerosols and its link to size-resolved chemical composition during spring and summer in Seoul, Korea, Atmospheric Chem. Phys., 20, 11245–11262, https://doi.org/10.5194/acp-20-11245-2020, 2020.

Kuang, Y., Huang, S., Xue, B., Luo, B., Song, Q., Chen, W., Hu, W., Li, W., Zhao, P., Cai, M., Peng, Y., Qi, J., Li, T., Wang, S., Chen, D., Yue, D., Yuan, B., and Shao, M.: Contrasting effects of secondary organic aerosol formations on organic aerosol hygroscopicity, Atmospheric Chem. Phys., 21, 10375–10391, https://doi.org/10.5194/acp-21-10375-2021, 2021.

Lide, D. R. (Ed.): CRC Handbook of Chemistry and Physics, 89th Edition, 89th edition., CRC Press, Boca Raton, 2736 pp., 2008.

Liu, D., Whitehead, J., Alfarra, M. R., Reyes-Villegas, E., Spracklen, D. V., Reddington, C. L., Kong, S., Williams, P. I., Ting, Y.-C., Haslett, S., Taylor, J. W., Flynn, M. J., Morgan, W. T., McFiggans, G., Coe, H., and Allan, J. D.: Black-carbon absorption enhancement in the atmosphere determined by particle mixing state, Nat. Geosci., 10, 184–188, https://doi.org/10.1038/ngeo2901, 2017.

Liu, D., Li, S., Hu, D., Kong, S., Cheng, Y., Wu, Y., Ding, S., Hu, K., Zheng, S., Yan, Q., Zheng, H., Zhao, D., Tian, P., Ye, J., Huang, M., and Ding, D.: Evolution of Aerosol Optical Properties from Wood Smoke in Real Atmosphere Influenced by Burning Phase and Solar Radiation, Environ. Sci. Technol., 55, 5677–5688, https://doi.org/10.1021/acs.est.0c07569, 2021.

Querry, M. R.: Optical Constants, US Army Chem. Res., Aberdeen Proving Ground, 418, 1985.

Shen, X. J., Sun, J. Y., Zhang, X. Y., Zhang, Y. M., Zhang, L., Che, H. C., Ma, Q. L., Yu, X. M., Yue, Y., and Zhang, Y. W.: Characterization of submicron aerosols and effect on visibility during a severe haze-fog episode in Yangtze River Delta, China, Atmos. Environ., 120, 307–316, https://doi.org/10.1016/j.atmosenv.2015.09.011, 2015.

Topping, D. O., McFiggans, G. B., and Coe, H.: A curved multi-component aerosol hygroscopicity model framework: Part 1 – Inorganic compounds, Atmospheric Chem. Phys., 5, 1205–1222, https://doi.org/10.5194/acp-5-1205-2005, 2005.